



MIT Open Access Articles

Silicon Detector Dark Matter Results from the Final Exposure of CDMS II

The MIT Faculty has made this article openly available. **Please share** how this access benefits you. Your story matters.

Citation	Agnese, R., Z. Ahmed, A. Anderson, S. Arrenberg, D. Balakishiyeva, R. Basu Thakur, D. Bauer, et al. "Silicon Detector Dark Matter Results from the Final Exposure of CDMS II." Physical Review Letters 111, no. 25 (December 2013). © 2013 American Physical Society
As Published	http://dx.doi.org/10.1103/PhysRevLett.111.251301
Publisher	American Physical Society
Version	Final published version
Accessed	Wed Sep 12 09:31:57 EDT 2018
Citable Link	http://hdl.handle.net/1721.1/85210
Terms of Use	Article is made available in accordance with the publisher's policy and may be subject to US copyright law. Please refer to the publisher's site for terms of use.
Detailed Terms	



Silicon Detector Dark Matter Results from the Final Exposure of CDMS II

R. Agnese,¹⁸ Z. Ahmed,¹ A. J. Anderson,⁴ S. Arrenberg,²⁰ D. Balakishiyeva,¹⁸ R. Basu Thakur,² D. A. Bauer,² J. Billard,⁴ A. Borgland,⁸ D. Brandt,⁸ P. L. Brink,⁸ T. Bruch,²⁰ R. Bunker,¹¹ B. Cabrera,¹⁰ D. O. Caldwell,¹⁵ D. G. Cerdeno,¹³ H. Chagani,¹⁹ J. Cooley,⁹ B. Cornell,¹ C. H. Crewdson,⁶ P. Cushman,¹⁹ M. Daal,¹⁴ F. Dejongh,² E. do Couto e Silva,⁸ T. Doughty,¹⁴ L. Esteban,¹³ S. Fallows,¹⁹ E. Figueroa-Feliciano,^{4,*} J. Filippini,¹ J. Fox,⁶ M. Fritts,¹⁹ G. L. Godfrey,⁸ S. R. Golwala,¹ J. Hall,⁵ R. H. Harris,¹² S. A. Hertel,⁴ T. Hofer,¹⁹ D. Holmgren,² L. Hsu,² M. E. Huber,¹⁶ A. Jastram,¹² O. Kamaev,⁶ B. Kara,⁹ M. H. Kelsey,⁸ A. Kennedy,¹⁹ P. Kim,⁸ M. Kiveni,¹¹ K. Koch,¹⁹ M. Kos,¹¹ S. W. Leman,⁴ B. Loer,² E. Lopez Asamar,¹³ R. Mahapatra,¹² V. Mandic,¹⁹ C. Martinez,⁶ K. A. McCarthy,⁴ N. Mirabolfathi,¹⁴ R. A. Moffatt,¹⁰ D. C. Moore,¹ P. Nadeau,⁶ R. H. Nelson,¹ K. Page,⁶ R. Partridge,⁸ M. Pepin,¹⁹ A. Phipps,¹⁴ K. Prasad,¹² M. Pyle,¹⁴ H. Qiu,⁹ W. Rau,⁶ P. Redl,¹⁰ A. Reisetter,¹⁷ Y. Ricci,⁶ T. Saab,¹⁸ B. Sadoulet,^{14,3} J. Sander,¹² K. Schneck,⁸ R. W. Schnee,¹¹ S. Scorza,⁹ B. Serfass,¹⁴ B. Shank,¹⁰ D. Speller,¹⁴ K. M. Sundqvist,¹⁴ A. N. Villano,¹⁹ B. Welliver,¹⁸ D. H. Wright,⁸ S. Yellin,¹⁰ J. J. Yen,¹⁰ J. Yoo,² B. A. Young,⁷ and J. Zhang¹⁹

(CDMS Collaboration)

¹*Division of Physics, Mathematics, and Astronomy, California Institute of Technology, Pasadena, California 91125, USA*

²*Fermi National Accelerator Laboratory, Batavia, Illinois 60510, USA*

³*Lawrence Berkeley National Laboratory, Berkeley, California 94720, USA*

⁴*Department of Physics, Massachusetts Institute of Technology, Cambridge, Massachusetts 02139, USA*

⁵*Pacific Northwest National Laboratory, Richland, Washington 99352, USA*

⁶*Department of Physics, Queen's University, Kingston, Ontario K7L 3N6, Canada*

⁷*Department of Physics, Santa Clara University, Santa Clara, California 95053, USA*

⁸*SLAC National Accelerator Laboratory/Kavli Institute for Particle Astrophysics and Cosmology, Menlo Park, California 94025, USA*

⁹*Department of Physics, Southern Methodist University, Dallas, Texas 75275, USA*

¹⁰*Department of Physics, Stanford University, Stanford, California 94305, USA*

¹¹*Department of Physics, Syracuse University, Syracuse, New York 13244, USA*

¹²*Department of Physics, Texas A&M University, College Station, Texas 77843, USA*

¹³*Departamento de Física Teórica and Instituto de Física Teórica UAM/CSIC, Universidad Autónoma de Madrid, 28049 Madrid, Spain*

¹⁴*Department of Physics, University of California, Berkeley, California 94720, USA*

¹⁵*Department of Physics, University of California, Santa Barbara, California 93106, USA*

¹⁶*Department of Physics, University of Colorado, Denver, Colorado 80217, USA*

¹⁷*Department of Physics, University of Evansville, Evansville, Indiana 47722, USA*

¹⁸*Department of Physics, University of Florida, Gainesville, Florida 32611, USA*

¹⁹*School of Physics and Astronomy, University of Minnesota, Minneapolis, Minnesota 55455, USA*

²⁰*Physics Institute, University of Zürich, Winterthurerstrasse 190, CH-8057, Switzerland*

(Received 4 May 2013; revised manuscript received 27 July 2013; published 16 December 2013)

We report results of a search for weakly interacting massive particles (WIMPs) with the silicon detectors of the CDMS II experiment. This blind analysis of 140.2 kg day of data taken between July 2007 and September 2008 revealed three WIMP-candidate events with a surface-event background estimate of $0.41_{-0.08}^{+0.20}(\text{stat})_{-0.24}^{+0.28}(\text{syst})$. Other known backgrounds from neutrons and ^{206}Pb are limited to <0.13 and <0.08 events at the 90% confidence level, respectively. The exposure of this analysis is equivalent to 23.4 kg day for a recoil energy range of 7–100 keV for a WIMP of mass $10 \text{ GeV}/c^2$. The probability that the known backgrounds would produce three or more events in the signal region is 5.4%. A profile likelihood ratio test of the three events that includes the measured recoil energies gives a 0.19% probability for the known-background-only hypothesis when tested against the alternative WIMP + background hypothesis. The highest likelihood occurs for a WIMP mass of $8.6 \text{ GeV}/c^2$ and WIMP-nucleon cross section of $1.9 \times 10^{-41} \text{ cm}^2$.

DOI: [10.1103/PhysRevLett.111.251301](https://doi.org/10.1103/PhysRevLett.111.251301)

PACS numbers: 95.35.+d, 14.80.Ly, 29.40.Wk, 95.55.Vj

There is now overwhelming evidence that the bulk of the matter in our Universe is in some nonluminous, non-baryonic form [1]. Weakly interacting massive particles (WIMPs) [2] form a leading class of candidates for this dark matter. Particles of this type would be produced thermally in the early Universe and are predicted by many theoretical extensions to the standard model of particle physics [1,3,4]. If WIMPs do constitute the dark matter in our Galaxy, they may be detectable through their elastic scattering from nuclei in terrestrial particle detectors [5]. Numerous experimental groups have sought to detect such scattering events using a wide variety of technologies [6].

The Cryogenic Dark Matter Search (CDMS) Collaboration identifies nuclear recoils (including those that would occur in WIMP interactions) using semiconductor detectors operated at 40 mK. These detectors use simultaneous measurements of ionization and nonequilibrium phonons to identify such events among the far more numerous background of electron recoils.

The low atomic mass of Si generally makes it a less sensitive target for spin-independent WIMP interactions relative to the larger coherent enhancement of the scattering cross section for heavy nuclei. On the other hand, the lower atomic mass of Si is advantageous in searches for WIMPs of relatively low mass ($\sim 10 \text{ GeV}/c^2$) due to more favorable scattering kinematics. New particles at such masses are generally disfavored in fits of models to precision electroweak data (e.g., Ref. [7]), but viable models in this regime do exist (e.g., Refs. [8,9]). Renewed interest in this mass range has been motivated by results from the DAMA/LIBRA [10], CoGeNT [11], and CRESST [12] experiments, which can be interpreted as evidence of low-mass WIMP scattering.

During 2003–2008 the collaboration operated CDMS II, an array of Ge and Si detectors located at the Soudan Underground Laboratory [13–19]. In its final configuration, the CDMS II array consisted of 30 Z-sensitive ionization and phonon (ZIP) detectors: 19 Ge ($\sim 239 \text{ g}$ each) and 11 Si ($\sim 106 \text{ g}$ each), for a total of $\sim 4.6 \text{ kg}$ of Ge and $\sim 1.2 \text{ kg}$ of Si. We discriminate nuclear recoils from background electron recoils using the ratio of ionization to phonon recoil energy (ionization “yield”). Electron recoils that occur within $\sim 10 \mu\text{m}$ of a detector surface can exhibit reduced ionization collection. These events are identified by phonon pulse-shape discrimination. Our overall misidentification rate of electron recoils is less than 1 in 10^6 .

We consider data from the Si detectors using the final four run periods of the full CDMS II detector installation acquired between July 2007 and September 2008. The Ge results from this data set have been described in previous publications [17,20]. Compared to Si data from the earlier CDMS II runs described in Ref. [21], these data benefit from improved analysis and calibration techniques. Of the 11 Si detectors, three were excluded from the WIMP-search analysis: two due to wiring failures that led to

incomplete collection of the ionization signal and one due to unstable response on one of its four phonon channels. Periods of poor performance, as identified by a series of Kolmogorov-Smirnov tests, were also excluded from analysis. After all such exclusions, the data collected by the eight Si detectors considered in this analysis represent a total exposure of 140.2 kg day prior to the application of the WIMP-candidate selection criteria.

The responses of these detectors to electron and nuclear recoils were calibrated using events from extensive exposures to ^{133}Ba and ^{252}Cf sources *in situ* at Soudan. Electron recoils from the former were used to empirically characterize and correct for the dependence of phonon pulse shape on event position and energy. The 356 keV gamma ray from the ^{133}Ba source has a $\sim 4.2 \text{ cm}$ attenuation length in Si, and thus the Si detectors generally do not show a clear line at 356 keV. Their energy scales were calibrated using 356 keV events with total energies shared between the Si detector and a neighboring detector.

WIMP-candidate events were identified by a series of selection criteria. All WIMP selection criteria were defined using calibration data plus WIMP search data in which events in and near the WIMP-candidate region were masked. Thus, WIMP candidates had no impact on the definition of the selection criteria. A WIMP candidate was required to have phonon and ionization signals above the noise in exactly one ZIP detector and to exhibit no coincident energy in the scintillating veto shield. Events in coincidence with the NuMI beam [22] were also vetoed. We demanded that any candidate event occur within the detector’s fiducial volume defined by requiring signal consistent with noise in the outer ionization electrode. The recoil energy of each candidate event had to lie below 100 keV and above a detector-dependent threshold ranging from 7 to 30 keV, chosen blindly using calibration data to keep the total expected leakage of bulk electron-recoil events into the nuclear-recoil band below 0.03 events. Candidate events were further required to lie $>4.5\sigma$ above the ionization channel noise as measured by randomly acquired triggers for each detector during each contiguous period of data taking ($\sim 24 \text{ h}$).

In yield, events were required to be within $+1.2\sigma$ and -1.8σ from the mean of the nuclear-recoil yield. Candidate events were also required to have phonon pulse timing consistent with a nuclear recoil. In order to take advantage of the fact that the timing parameters are better measured at high energies, the phonon timing data-selection cut was optimized in three energy bins: 7–20, 20–30, and 30–100 keV [23]. Figure 1 shows the nuclear-recoil efficiency, i.e., the estimated fraction of nuclear recoils at a given energy that would be accepted by these signal criteria, measured using nuclear recoils from ^{252}Cf calibration. The abrupt changes in efficiency are due to the different detector thresholds and changes to the timing cuts in the three energy bins. Signal acceptance was measured using nuclear recoils from ^{252}Cf calibration. After applying

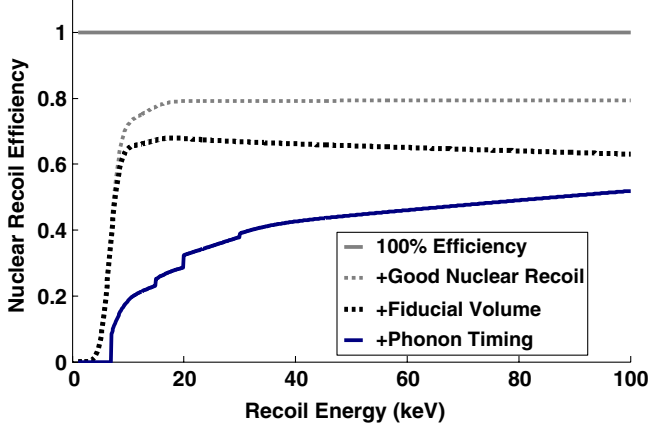


FIG. 1 (color online). Nuclear-recoil efficiency as a function of recoil energy after application of each selection criterion is shown. Each curve from top to bottom shows the cumulative effect of successive cuts on the data, with the second curve from the top (gray dashed) encompassing all data-quality cuts, trigger, and ionization threshold efficiencies, and the nuclear-recoil yield band efficiency as measured on ^{252}Cf neutrons. The third curve (black dashed) adds the ionization radial cut to the above. The bottom curve (solid blue) adds both the phonon timing criteria and the recoil-energy thresholds, and hence shows the overall efficiency of this analysis. The abrupt drops in acceptance at low recoil energies reflect the elevated energy thresholds chosen for some detectors.

all selection criteria, the exposure of this analysis is equivalent to 23.4 kg day over a recoil energy range of 7–100 keV for a WIMP of mass $10 \text{ GeV}/c^2$.

Neutrons from cosmogenic or radioactive processes can produce nuclear recoils that are indistinguishable from those from an incident WIMP. Simulations of the rates and energy distributions of these processes using GEANT4 [24] lead us to expect <0.13 false candidate events (90% confidence level) in the Si detectors from neutrons for this exposure with all efficiencies included.

A greater source of background is the misidentification of surface electron recoils, which may suffer from reduced ionization yield and thus contribute events to the WIMP-candidate region; these events are termed “leakage events.” Prior to looking at the WIMP-candidate region (unblinding), the expected leakage was estimated using the rate of single-scatter events with yields consistent with nuclear recoils from a previously unblinded Si data set [25] and the rejection performance of the timing cut measured on low-yield multiple-scatter events from ^{133}Ba calibration data. Two detectors used in this analysis were located at the end of detector stacks, so scatters on their outer faces could not be tagged as multiple scatters. The rate of surface events on the outer faces of these two detectors were estimated using their single-scatter rates from a previously unblinded data set presented in Ref. [25] and the multiples-singles ratio on the interior detectors. The final preunblinding estimate for misidentified surface

electron-recoil event leakage into the signal band in the eight Si detectors was $0.47^{+0.28}_{-0.17}$ (stat) events. This initial leakage estimate informed the decision to unblind. After unblinding, we developed a Bayesian estimate of the rate of misidentified surface events based upon the performance of the phonon timing cut measured using events near the WIMP-search signal region [21,25]. Multiple-scatter events below the electron-recoil ionization-yield region from both ^{133}Ba calibration and the WIMP-search data were used as inputs to this model. Because the WIMP-search sample is sparser compared to the calibration data, the combined estimates are more heavily weighted towards the calibration data leakage estimates. Additionally, the leakage estimate is corrected for the fact that the fraction of singles passing the timing cut is higher than the fraction of multiples by a factor of $1.7^{+0.8}_{-0.6}$, as measured on low-yield events outside of the nuclear-recoil band. The systematic uncertainty on the leakage estimate comes from the uncertainty on this scale factor, the choice of prior in the Bayesian analysis, and the method used to reweigh the energy distribution of surface events from calibration data to reflect the distribution in WIMP search data. The final model predicts an updated surface-event leakage estimate of $0.41^{+0.20}_{-0.08}$ (stat) $^{+0.28}_{-0.24}$ (syst) misidentified surface electron-recoil events in the eight Si detectors. Classical confidence intervals provided similar estimates [26].

After all WIMP-selection criteria were defined, the signal regions of the Si detectors were unblinded on December 25, 2012. Three WIMP-candidate events were observed, with recoil energies of 8.2, 9.5, and 12.3 keV, on March 14, July 1, and September 6 of 2008, respectively. Two events were observed in detector 3 of tower 4, and the third was observed in detector 3 of tower 5. These detectors were near the middle of their respective tower stacks. Figure 2 illustrates the distribution of events in and near the signal region of the WIMP-search data set before (top) and after (bottom) application of the phonon timing criterion. Figure 3 shows an alternate view of these events expressed in “normalized” versions of yield and timing that are transformed so that the WIMP acceptance regions of all detectors coincide.

After unblinding, extensive checks of the three candidate events revealed no data quality or analysis issues that would invalidate them as WIMP candidates. The signal to noise on the ionization channel for the three events (ordered in increasing recoil energy) was measured to be 6.7σ , 4.9σ , and 5.1σ . A study on possible leakage into the signal band due to ^{206}Pb recoils from ^{210}Po decays found the expected leakage to be negligible with an upper limit of <0.08 events at the 90% confidence level. The energy distribution of the ^{206}Pb background was constructed using events in which a coincident α particle was detected in a detector adjacent to one of the eight Si detectors used in this analysis.

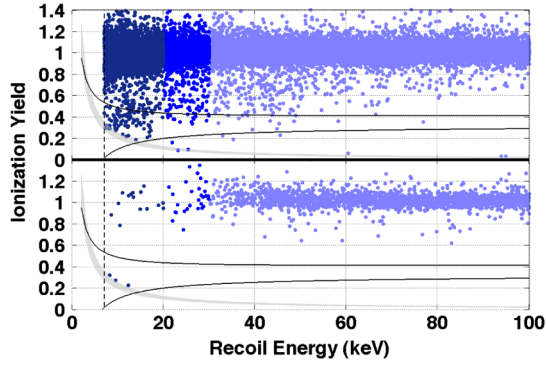


FIG. 2 (color online). Ionization yield versus recoil energy in all detectors included in this analysis for events passing all signal criteria except (top) and including (bottom) the phonon timing criterion. The curved black lines indicate the signal region (-1.8σ and $+1.2\sigma$ from the mean nuclear-recoil yield) between 7 and 100 keV recoil energies for detector 3 in tower 4, while the gray band shows the range of charge thresholds across detectors. Electron recoils in the detector bulk have yield near unity. The data are colored (dark to light gray) to indicate recoil energy ranges of 7–20, 20–30, and 30–100 keV to aid the interpretation of Fig. 3.

This result constrains the available parameter space of WIMP dark matter models. We compute upper limits on the WIMP-nucleon scattering cross section using Yellin’s optimum interval method [27]. We assume a WIMP mass density of $0.3 \text{ GeV}/c^2/\text{cm}^3$, a most probable WIMP

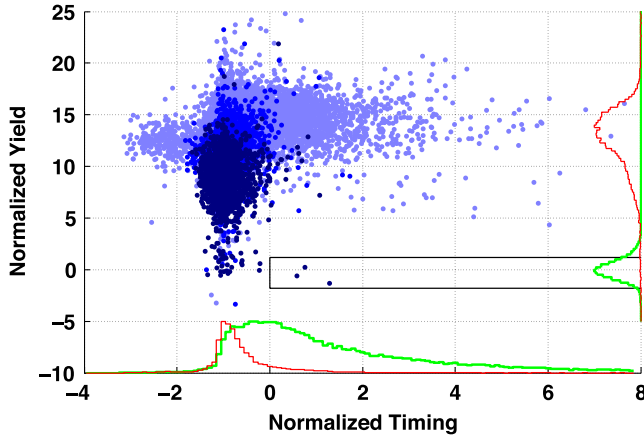


FIG. 3 (color online). Normalized ionization yield (standard deviations from the nuclear-recoil band centroid) versus normalized phonon timing parameter (normalized such that the median of the surface-event calibration sample is at -1 and the cut position is at 0) for events in all detectors from the WIMP-search data set passing all other selection criteria. The black box indicates the WIMP-candidate region. The data are colored (dark to light gray) to indicate recoil energy ranges of 7–20, 20–30, and 30–100 keV. The thin red curves on the bottom and right axes are the histograms of the data, while the thicker green curves are the histograms of nuclear recoils from ^{252}Cf calibration data; both are normalized to have the same arbitrary peak value.

velocity with respect to the Galaxy of 220 km/s, a mean circular velocity of Earth with respect to the Galactic center of 232 km/s, a Galactic escape velocity of 544 km/s [28], and the Helm form factor [29]. The effect of an annual modulation of the $10 \text{ GeV}/c^2$ WIMP rate found by integrating over the specific data-taking periods for this analysis with the above assumptions introduces a $<2\%$ shift downward in the cross sections of our results and is thus neglected. Figure 4 shows the derived upper limits on the spin-independent WIMP-nucleon scattering cross section at the 90% C.L. from this analysis and a selection of other recent results. The present data set set an upper limit of $2.4 \times 10^{-41} \text{ cm}^2$ for a WIMP of mass $10 \text{ GeV}/c^2$. We are completing the calibration of the nuclear-recoil energy scale using the Si-neutron elastic scattering resonant feature in the ^{252}Cf exposures. This study indicates that our reconstructed energy may be 10% lower than the true recoil energy, which would weaken the upper limit slightly. Below $20 \text{ GeV}/c^2$, the change is well approximated by shifting the limits parallel to the mass axis by $\sim 7\%$, making the limits weaker at low masses. In addition, neutron calibration multiple-scattering effects improve the response to WIMPs, thus shifting the upper limit down to a lower cross-section axis and making the limits stronger by $\sim 5\%$.

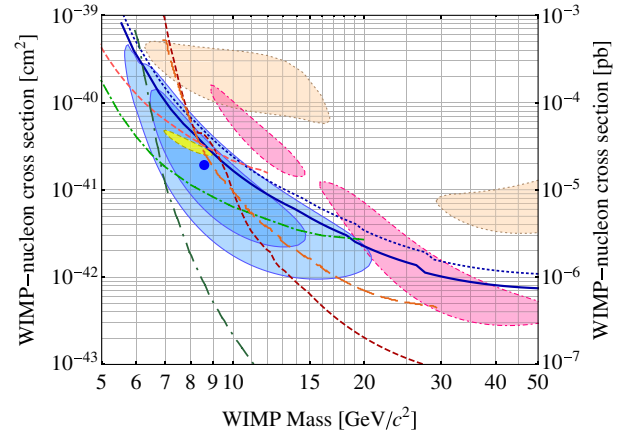


FIG. 4 (color online). Experimental upper limits (90% confidence level) for the WIMP-nucleon spin-independent cross section as a function of WIMP mass. We show the limit obtained from the exposure analyzed in this work alone (blue dotted line), and combined with the CDMS II Si data set reported in Refs. [21,25] (blue solid line). Also shown are limits from the CDMS II Ge standard [17] and low-threshold [20] analysis (dark and light dashed red), EDELWEISS low-threshold [30] (long-dashed orange), XENON10 S2 only [31] (dash-dotted green), and XENON100 [32] (long-dash-dotted green). The filled regions identify possible signal regions associated with data from CoGeNT [33] (dashed yellow, 90% C.L.), DAMA/LIBRA [10,34] (dotted tan, 99.7% C.L.), and CRESST [12,35] (dash-dotted pink, 95.45% C.L.) experiments. The 68% and 90% C.L. solid contours for a possible signal from these data alone are shown in light blue. The blue dot shows the maximum likelihood point at $(8.6 \text{ GeV}/c^2, 1.9 \times 10^{-41} \text{ cm}^2)$.

A model of our known backgrounds including both energy and expected rate distributions was constructed for each detector and experimental run for each of the three backgrounds considered: surface electron recoils, neutron backgrounds, and ^{206}Pb recoils. Simulations of our background model yield a 5.4% probability of a statistical fluctuation producing three or more events in our signal region.

This model of our known backgrounds was used to investigate the data in the context of a WIMP + background hypothesis. We performed a profile likelihood analysis, including the event energies, in which the background rates were treated as nuisance parameters and the WIMP mass and cross section were the parameters of interest. We profiled over probability distribution functions of the rate for each of our known backgrounds. The highest likelihood was found for a WIMP mass of 8.6 GeV/ c^2 and a WIMP-nucleon cross section of 1.9×10^{-41} cm 2 . The goodness-of-fit test of this WIMP + background hypothesis results in a p value of 68%, while the background-only hypothesis fits the data with a p value of 4.5%. A profile likelihood ratio test finds that the data favor the WIMP + background hypothesis over our background-only hypothesis with a p value of 0.19%. Though this result favors a WIMP interpretation over the known-background-only hypothesis, we do not believe this result rises to the level of a discovery.

Figure 4 shows the resulting best-fit region from this analysis (68% and 90% confidence level contours) on the WIMP-nucleon cross section versus WIMP mass plane. The 90% C.L. exclusion regions from CDMS II's Ge and Si analyses and EDELWEISS low-threshold analysis cover part of this best-fit region, but the results are overall statistically compatible. While there is some tension with the upper limits from the XENON10 experiment, the XENON100 experiment significantly constrains this parameter space under standard assumptions about the WIMP velocity distribution and WIMP-nucleus interactions. Additional, planned studies of these CDMS II Si data with reduced threshold may provide additional insight into a WIMP interpretation of these data. Future experiments with Si-based detectors that would be sensitive to WIMPs in this region of parameter space are also under consideration by the SuperCDMS Collaboration.

The CDMS Collaboration gratefully acknowledges the contributions of numerous engineers and technicians; we would like to especially thank Dennis Seitz, Jim Beaty, Bruce Hines, Larry Novak, Richard Schmitt, and Astrid Tomada. In addition, we gratefully acknowledge assistance from the staff of the Soudan Underground Laboratory and the Minnesota Department of Natural Resources. This work is supported in part by the National Science Foundation (Grants No. AST-9978911, No. NSF-0847342, No. NSF-1151869, No. PHY-0542066, No. PHY-0503729, No. PHY-0503629, No. PHY-0503641, No. PHY-0504224,

No. PHY-0705052, No. PHY-0801708, No. PHY-0801712, No. PHY-0802575, No. PHY-0847342, No. PHY-0855299, No. PHY-0855525, No. PHY-1102795, and No. PHY-1205898), by the Department of Energy (Contracts No. DE-AC03-76SF00098, No. DE-FG02-92ER40701, No. DE-FG02-94ER40823, No. DE-FG03-90ER40569, No. DE-FG03-91ER40618, and No. DE-SC0004022), by the Swiss National Foundation (SNF Grant No. 20-118119), by NSERC Canada (Grants No. SAPIN 341314 and No. SAPPJ 386399), and by MULTIDARK Grants No. CSD2009-00064 and No. FPA2012-34694. Fermilab is operated by Fermi Research Alliance, LLC, under Contract No. De-AC02-07CH11359, while SLAC is operated under Contract No. DE-AC02-76SF00515 with the United States Department of Energy.

*Corresponding author.

enectali@mit.edu

- [1] G. Bertone, D. Hooper, and J. Silk, *Phys. Rep.* **405**, 279 (2005).
- [2] G. Steigman and M. S. Turner, *Nucl. Phys.* **B253**, 375 (1985).
- [3] B. W. Lee and S. Weinberg, *Phys. Rev. Lett.* **39**, 165 (1977).
- [4] G. Jungman, M. Kamionkowski, and K. Griest, *Phys. Rep.* **267**, 195 (1996).
- [5] M. W. Goodman and E. Witten, *Phys. Rev. D* **31**, 3059 (1985).
- [6] G. Bertone and J. Silk, *Particle Dark Matter: Observations, Models, and Searches* (Cambridge University Press, Cambridge, England, 2010).
- [7] E. A. Baltz and P. Gondolo, *J. High Energy Phys.* **10** (2004) 052; L. Roszkowski, R. Ruiz de Austri, and R. Trotta, *J. High Energy Phys.* **07** (2007) 075.
- [8] A. Bottino, F. Donato, N. Fornengo, and S. Scopel, *Phys. Rev. D* **69**, 037302 (2004).
- [9] D. E. Kaplan, M. A. Luty, and K. M. Zurek, *Phys. Rev. D* **79**, 115016 (2009); T. Cohen and K. M. Zurek, *Phys. Rev. Lett.* **104**, 101301 (2010).
- [10] R. Bernabei *et al.* (DAMA Collaboration), *Eur. Phys. J. C* **67**, 39 (2010).
- [11] C. E. Aalseth *et al.* (CoGeNT Collaboration), *Phys. Rev. Lett.* **106**, 131301 (2011).
- [12] G. Angloher *et al.* (CRESST Collaboration), *Eur. Phys. J. C* **72**, 1971 (2012).
- [13] D. Akerib *et al.* (CDMS Collaboration), *Phys. Rev. D* **72**, 052009 (2005).
- [14] D. S. Akerib *et al.* (CDMS Collaboration), *Phys. Rev. Lett.* **93**, 211301 (2004).
- [15] D. S. Akerib *et al.* (CDMS Collaboration), *Phys. Rev. Lett.* **96**, 011302 (2006).
- [16] Z. Ahmed *et al.* (CDMS Collaboration), *Phys. Rev. Lett.* **102**, 011301 (2009).
- [17] Z. Ahmed *et al.* (CDMS Collaboration), *Science* **327**, 1619 (2010).
- [18] Z. Ahmed *et al.* (CDMS Collaboration), *Phys. Rev. D* **81**, 042002 (2010).

- [19] Z. Ahmed *et al.* (CDMS Collaboration), *Phys. Rev. Lett.* **103**, 141802 (2009).
- [20] Z. Ahmed *et al.* (CDMS Collaboration), *Phys. Rev. Lett.* **106**, 131302 (2011).
- [21] R. Agnese *et al.* (CDMS Collaboration), *Phys. Rev. D* **88**, 031104 (2013).
- [22] K. Anderson *et al.*, Fermilab Technical Report No. FERMILABDESIGN-1998-01, 1998.
- [23] K. A. McCarthy, Ph.D. thesis, Massachusetts Institute of Technology, 2013.
- [24] J. Allison *et al.*, *IEEE Trans. Nucl. Sci.* **53**, 270 (2006).
- [25] J.P. Filippini, Ph.D. thesis, University of California, Berkeley, 2008.
- [26] I. Ruchlin and R.W. Schnee, *Nucl. Instrum. Methods Phys. Res., Sect. A* **664**, 336 (2012).
- [27] S. Yellin, *Phys. Rev. D* **66**, 032005 (2002).
- [28] M. C. Smith, G. Ruchti, A. Helmi, R. Wyse, J. Fulbright *et al.*, *Mon. Not. R. Astron. Soc.* **379**, 755 (2007).
- [29] J.D. Lewin and P.F. Smith, *Astropart. Phys.* **6**, 87 (1996).
- [30] E. Armengaud *et al.* (EDELWEISS Collaboration), *Phys. Rev. D* **86**, 051701 (2012).
- [31] J. Angle *et al.* (XENON10 Collaboration), *Phys. Rev. Lett.* **107**, 051301 (2011); **110**, 249901 (2013).
- [32] E. Aprile *et al.* (XENON100 Collaboration), *Phys. Rev. Lett.* **109**, 181301 (2012).
- [33] C. E. Aalseth *et al.* (CoGeNT Collaboration), *Phys. Rev. D* **88**, 012002 (2013).
- [34] C. Savage, G. Gelmini, P. Gondolo, and K. Freese, *J. Cosmol. Astropart. Phys.* **04** (2009) 010.
- [35] A. Brown, S. Henry, H. Kraus, and C. McCabe, *Phys. Rev. D* **85**, 021301 (2012).